VECTOR SPECTRUM AND COLOR SCREENING IN TWO COLOR QCD AT NONZERO T AND μ

BARTOLOMÉ ALLÉS
Dipartimento di Fisica, Università di Milano–Bicocca and INFN Sezione di Milano, I-20126 Milano, Italy

MASSIMO D'ELIA
Dipartimento di Fisica, Università di Genova and INFN Sezione di Genova, I-16146 Genova, Italy

MARIA- PAOLA LOMBARDO
INFN Sezione di Padova, and Laboratori di Frascati, I-00044 Frascati, Italy

MICHELE PEPE
Laboratoire de Physique Théorique, Université de Paris XI, 91405 Orsay Cedex, France and ITP, University of Bern, CH-3012 Bern, Switzerland

We discuss a few aspects of the phase diagram of two color lattice QCD: we investigate the long distance screening analyzing the behavior of the interquark potential at large distances; we present a first set of results for vector mesons and diquarks; we note similarities and differences between features at high temperature and high baryon density.

1 Introduction

In this note we report on a numerical investigation of the phase diagram of two color QCD in the temperature–chemical potential plane. In this theory, the fermion determinant is positive at nonzero baryon density [1,2] and lattice simulations are possible.

Several studies of this model have already appeared [3,4,5] and, in particular, the phase diagram in the temperature–density plane at nonzero bare quark mass has been studied in some detail [6,7,8]. There are three different phases: a hadronic phase with confinement and spontaneous (approximate) chiral symmetry breaking, a superfluid phase with diquark condensation and a plasma phase. For a nonzero quark mass and a zero diquark source, which is our case, the superfluid line is a bonafide phase transition, the other lines are either crossover or first order transitions. It has been shown [6,8] that, for some values of μ, either $\langle\bar{\psi}\psi\rangle$ or $\langle\psi\psi\rangle$ are non–monotonic function of temperature. An earlier, sketchy proposal of the phase diagram [7] suggests a non–monotonic behavior for the diquark condensate. Such behaviors are rather common in

condensed matter (e.g. superconductors) but unusual in particle physics: that adds to the interest of two color QCD.

Our aim is to characterize the various phases and their associated phenomena by continuing the study of the spectrum of mesons and diquarks and by exploring in detail the behavior of purely gluonic observables.

Here we will discuss only a few aspects of our study: the behavior of the Polyakov loop and its correlators, and a first set of results for the vector meson and diquark spectrum. A complete presentation, which will include topological [9] and thermodynamics results, will appear in a future publication [10].

2 The simulations

Numerical simulations of two color QCD with eight continuum flavors have been carried out on a $14^3 \times 6$ lattice by an HMD algorithm [2], for several values of temperatures, masses and chemical potentials. We have considered chemical potentials between zero and the lattice saturation and temperatures ranging from $T \simeq 0$ to $T > T_c$.

Typically, we have run for O(10000) MD steps, with dt = .02 and taking measures every 40 steps.

A few test runs were performed with dt = .04 and dt = .08 in order to check that discretization errors are small at dt = .02. The accuracy of the inversion of the Dirac operator has been tested by use of the lattice Ward identity.

3 Color screening

It is interesting to remark that for two color QCD the Polyakov loop P is a real quantity: hence, the Polyakov loop correlator defining the strength of the quark-quark interaction $\langle PP(R)\rangle/\langle P\rangle^2$, is the same as the quark–antiquark one $\langle PP^\dagger(R)\rangle/|\langle P\rangle|^2$. This property remains true also at $\mu \neq 0$.

Note however, that this is the only special feature of the Polyakov loop and its correlators in two color QCD: all of the discussion can be carried out for a generic number of color N_c. For this reason, it might well be that some of the finding presented here carry over to real QCD.

The confined phase in the quenched approximation is characterized by an interquark static potential which rises linearly at any distance $\lim_{R\to\infty} V(R) \propto \sigma R$, σ being the string tension.

When quark degrees of freedom start to be dynamical a new phenomenon takes place. The color flux tube between two static quarks can now break by pair production of dynamical quarks popping out of the vacuum and screening

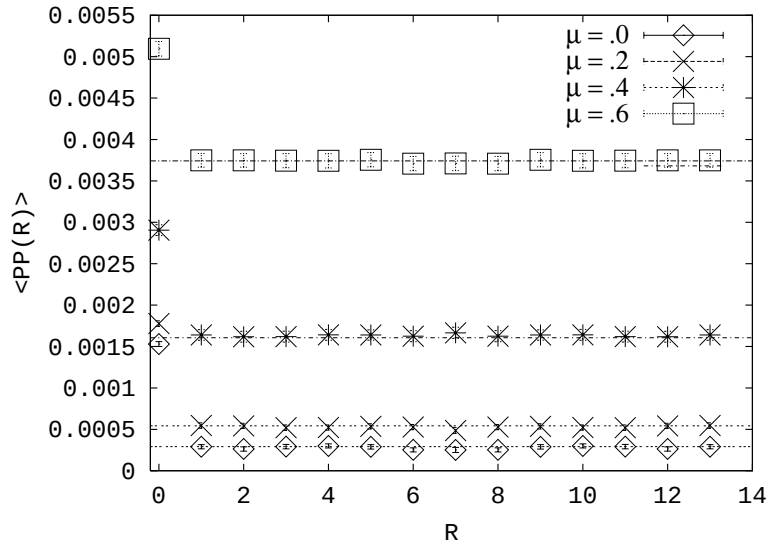

Figure 1. Polyakov loop correlation for $\beta = 1.5$ and various chemical potentials: screening and string breaking grow rapidly around μ_c. The horizontal lines are drawn in correspondence of $\langle P \rangle^2$, demonstrating the cluster property of the correlators.

the two static sources (string breaking): $Q\bar{Q} \to (Q\bar{q})(q\bar{Q})$. The potential does not rise indefinitely anymore but flattens out at sufficiently large distance R_0.

String breaking in the hadronic phase has been observed at a moderately high temperature [11], and it has also been suggested that the real particles present in a dense system further favors the breaking of the string [12].

In the following, we will study the behaviour of the interquark potential as a function of μ, and we will contrast its behaviour with that observed as a function of temperature.

Consider the Polyakov loop at spatial coordinates $\vec{n} = (n_1, n_2, n_3)$

$$P(\vec{n}) = (1/N_c) Tr \prod_{\tau=0}^{N_\tau - 1} U_0(\vec{n}, \tau) \; . \tag{1}$$

We average $P(\vec{n})$ on spatial planes to build:

$$P_3(n_3) = (1/{N_s}^2) \sum_{n_1, n_2 = 1}^{N_s} P(n_1, n_2, n_3) \tag{2}$$

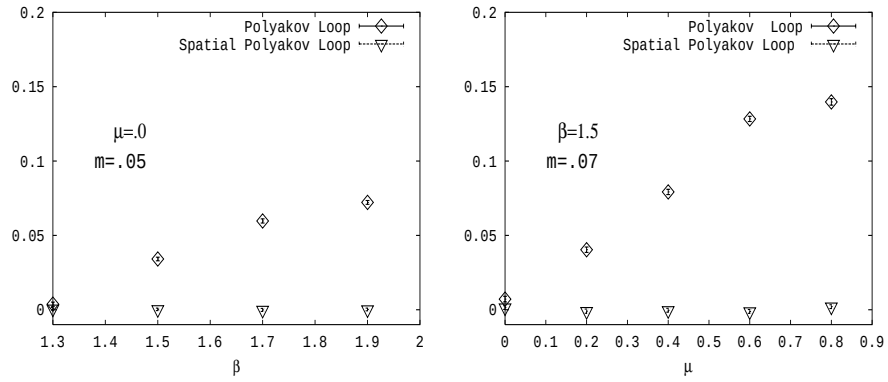

Figure 2. Polyakov loop, and spatial Polyakov loop, as a function of β (left) and μ

P_1 and P_2 are similarly defined.

By use of $P_i(n_i)$ we finally arrive at the zero-th momentum projected correlation function of the Polyakov line

$$\langle PP^\dagger(R)\rangle = \frac{1}{3N_s}\sum_{i=1}^{3}\sum_{n_i=1}^{N_s}\langle P_i(n_i)P_i^\dagger(n_i+R)\rangle\ . \tag{3}$$

In Fig. 1 we show the results for the Polyakov loop correlators at various values of the chemical potential. At high chemical potential we observe the expected enhanced screening, since the correlation functions approach a constant value at large distance. The gap between the plateaux at $\mu = 0.2$ and $\mu = 0.4$ in Fig. 1 suggests the passage to a deconfined phase. We have then a direct evidence of the effect of the chemical potential on the gauge fields.

We note that the trend with chemical potential closely resembles that observed with temperature [11]: in both cases we have signals of deconfinement.

In Fig. 2 the dependence of the Polyakov loop on μ (left hand side) and on T (right hand side) is contrasted with that of the spatial Polyakov loop, superimposed in the same plots. Again we note the similarity between the behaviour at high temperature and that at high density : in both cases, only the temporal loop is affected.

These results provide a direct observation of long range screening in a dense gauge system, obtained from a first principle study of the model, further confirming other observations[4]. They are thus providing an important confirmation of the standard expectation of the structure of a dense medium.

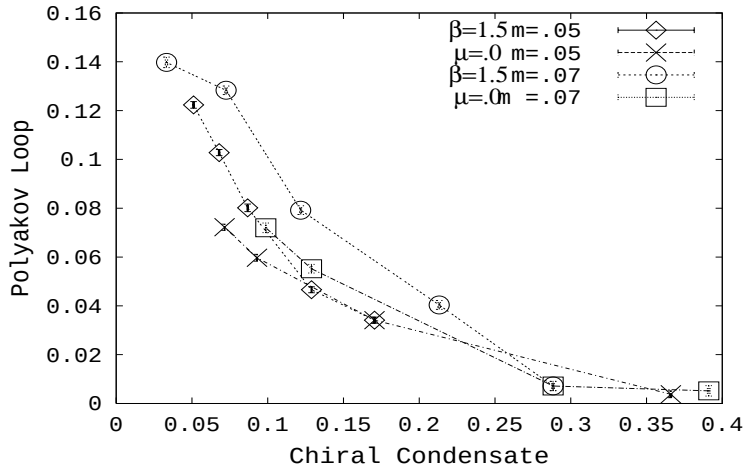

Figure 3. Polyakov loop versus the chiral condensate

A more detailed analysis can give us more information on the screening properties. We note that some theoretical guidance can also be offered by low energy effective string models [13], which provide the following expression (simplified for the sake of the present discussion) for the point-to-point correlators:

$$\langle PP^{\dagger}(R)\rangle = \alpha e^{-\sigma_0 R N_t} + (N_c N_f)^2 \beta e^{-2\sigma_0 R_0 N_t} \ . \tag{4}$$

The above equation shows the expected exponential dependence on the breaking length R_0, hence on the mass scale, and we also note the dynamical factors α and β. It is then reasonable to assume that they depend on temperature and density: we will address this point in our future publication.

Finally, in Fig. 3 we study the correlation between $|\langle P\rangle|$ and $\langle\bar{\psi}\psi\rangle$ by plotting one versus the other. We plot there two sets of data: firstly, those obtained at fixed $\beta = 1.5$, and variable μ. Secondly, those at $\mu = 0$, and variable β. We see that chiral condensate and Polyakov loop are well correlated, for both data sets , and that the Polyakov loop looks consistently larger for the first data set , $\beta = 1.5, \mu \neq 0$, supporting the idea that a finite density of real particles further favors string breaking [12].

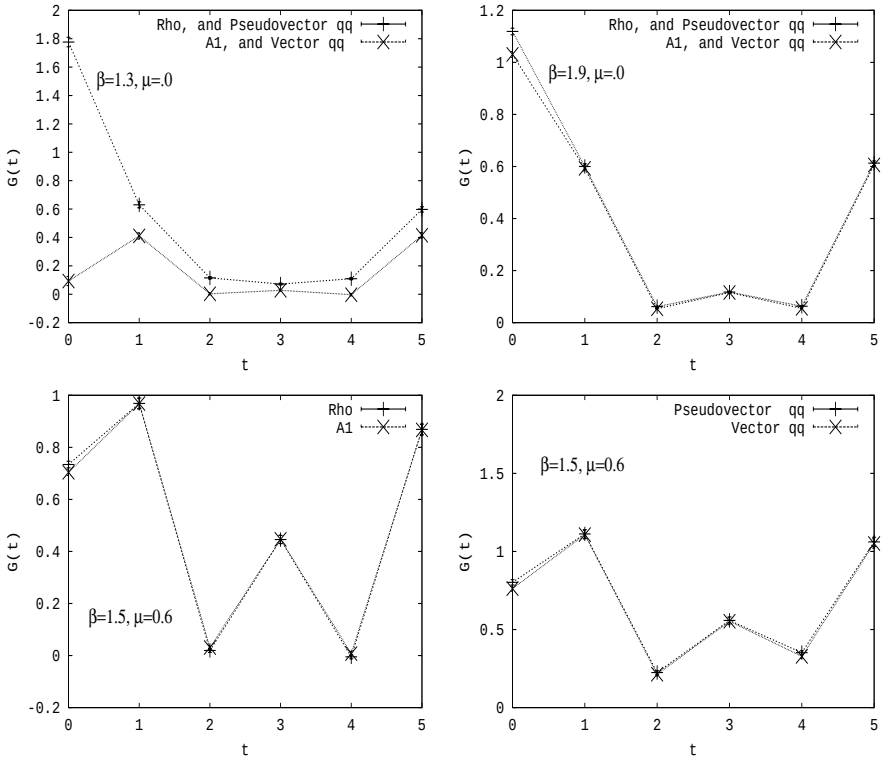

Figure 4. Vector mesons and diquarks propagators $G(t)$ as a function of Euclidean time t. Upper, left: vector and pseudovector meson propagators in the hadronic phases. Vector diquarks are degenerate. Upper, right: as in left part of the diagram, but in the plasma phase: chiral symmetry is restored. Lower, left: vector mesons at high density; the propagators are degenerate, as it happens at high T, but chiral symmetry is still broken. Note anomalous spectral behaviour. Lower, right: vector diquarks at high density; time reversal symmetry is broken, and we note possible hints of vector condensation

4 The vector sector

The vector meson ($\bar{q}\gamma_i q$) and diquark ($q\gamma_i q$) and antidiquark ($\bar{q}\gamma_i \bar{q}$) propagators at $\mu = 0$ are constructed from the quark propagator, as explained in early work [2] for the scalar spectrum, modulo the inclusion of the appropriate γ matrix (or, rather, of its staggered fermion representation).

From the Pauli–Gursey symmetry of the SU(2) Action, the exact degen-

eracy of the vector (V) meson propagator with the pseudovector (PV) diquark propagator follows, as well as that of the pseudovector meson propagator with the vector diquark propagator. Analogous degeneracies have been noted in the scalar sector [2].

Finite density spectroscopy analysis has been already introduced and discussed [14]. The following symmetries should hold true in the ensemble:

$$G(t) = G(T-t) \qquad \text{for mesons} \tag{5}$$

$$G(t,\mu) = G(T-t,-\mu) \qquad \text{for diquarks} \tag{6}$$

In addition to that, remember that staggered mesons contain states with different lattice parity (the 'oscillating' channel): for instance, the vector meson contains both the ρ and the B particle, while the pseudovector contains the A1 and again the ρ:

$$G_V(t) = a(e^{(-m_\rho t)} + e^{m_\rho (T-t)}) + (-1)^t b(e^{(-m_B t)} + e^{m_B (T-t)}) \tag{7}$$

$$G_{PV}(t) = a(e^{(-m_{A1} t)} + e^{m_{A1} (T-t)}) + (-1)^t b(e^{(-m_\rho t)} + e^{m_\rho (T-t)}) \tag{8}$$

Since mesons do not 'feel' the effects of the chemical potential the masses of the forward and backward propagating meson states are identical.

For $\mu \neq 0$ we expect different forward and backward masses in the diquark channels, reflecting the different backward and forward propagations in the dense medium. The occurrence of condensation, in either channel, should be signaled by the appearance of a constant term at large distance.

Let us look now at the diagrams, Fig.4: the upper left diagram shows the vector and pseudovector meson propagators at low temperature, zero chemical potential. We have verified that they are degenerate with the vector diquarks of opposite parity. By increasing the temperature we observe chiral symmetry restoration in the vector channel (Fig.4, upper right diagram): all of the four vector states (mesons and diquarks) are now degenerate. At nonzero density mesons and diquarks with opposite parity are no longer degenerate, as anticipated. Let us follow independently mesons and diquarks then.

In Fig.4 , left lower diagram, we see the vector and pseudovector mesons for $\mu > \mu_c$: they are degenerate, as it happens at high T: of course this does not signal chiral symmetry restoration , since chiral symmetry is still broken by the diquark condensate. Simply, it tells us that the chiral condensate, which is responsible for the difference between these two propagators, is now zero. This is the same which happened with scalars. We observe also an important difference : the oscillating componenent is increased, as if the B particle contribution were more important at high density. This might indicate a significant difference of the spectral functions at high temperature and density,

suggesting that the spectral concentration of the ρ decreases at high density in comparison to that of the B meson.

One last remark concerns the behavior of vector diquarks: in addition to the expected asymmetry, we observe (Fig.4 , right lower diagram) a behaviour which is not inconsistent with a possible plateau. Obviously, also a very low mass can mimick this behaviour, and all the usual caveat apply to this observation : first of all we should study colder lattices, where condensation phenomena are more prominent. Secondly, we should check finite size scaling. If this trend were to persist for a range of lattice volumes then it could be interpreted as evidence for the predicted [5] vector condensation.

5 Summary

We have observed enhanced screening and string breaking in the critical region for chiral symmetry. We have shown that chiral condensate and screening properties are correlated both at finite temperature and finite density. These observations suggest that the (pseudo)critical line for chiral condensate and confinement run close to each other in the phase diagram of two color QCD. Moreover we noticed that, at comparable values of chiral condensate, string breaking is slightly more pronounced at finite density, and low temperature, than at zero density and finite temperature. This supports the view that recombination with real quarks in a dense system favors deconfinement [12].

We have observed exact degeneracies in the vector sector of the spectrum. We have studied the pattern of chiral symmetry for vector mesons and diquarks at finite temperature and density. Our results show a peculiar behaviour in the meson vector sector at high density, noticeably different from that at high temperature: spectral concentration of the B particle seems dominating over the ρ, while at high temperature the opposite holds true. Finally we have noted possible hints of vector condensation in the diquark sector.

One final remarks concerns the possibility to use two color QCD to test methods for simulating QCD at nonzero density. Some experiments with the Glasgow reweighting have already been performed [15], while test of the analytic continuation from imaginary chemical potential [16] are in progress [17].

Acknowledgments

We wish to thank J.T. Lenaghan, F. Sannino, W. Schäfer, K. Splittorff and D. Toublan for interesting conversations. This work has been partially supported by MIUR. M.P. thanks the European Union Human Potential Program (contract HPRN-CT-2000-00145, Lattice QCD).

References

1. E. Dagotto, F. Karsch and A. Moreo, Phys. Lett. 169B (1986) 421; E.Dagotto, A.Moreo and U.Wolff, Phys. Lett. 186B (1987) 395.
2. S.J. Hands, J. B. Kogut, M.-P. Lombardo, S.E. Morrison, Nucl.Phys. B558 (1999) 327.
3. J.B. Kogut, M. A. Stephanov, D. Toublan, J.J.M. Verbaarschot, Nucl.Phys.B 582 (2000) 477; K. Splittorff, D. Toublan, J.J.M. Verbaarschot, hep-ph/0204076; J. B. Kogut, D. Toublan, D.K. Sinclair, Phys.Lett.B514 (2001) 77 ;K. Splittorff, D. Toublan, J.J.M. Verbaarschot, Nucl.Phys.B620 (2002) 290; J.B. Kogut, D.K. Sinclair, S.J. Hands, S.E. Morrison; Phys.Rev.D64 (2001) 094505; E. Bittner, M.-P. Lombardo, H. Markum, R. Pullirsch, Nucl.Phys.Proc.Suppl.94 (2001) 445; R. Aloisio, V. Azcoiti, G. Di Carlo, A. Galante, A.F. Grillo , Phys.Lett.B 493 (2002) 189.
4. S. Muroya, A. Nakamura, C. Nonaka, nucl-th/0111082; Y. Liu, O. Miyamura, A. Nakamura, T. Takaishi in *Non-perturbative methods and lattice QCD* p. 132; S. Muroya, A. Nakamura and C. Nonaka, hep-lat/0208006;M-P Lombardo, hep-lat/9907025.
5. F. Sannino and W. Schaefer , Phys.Lett.B527 (2002) 142; J.T. Lenaghan, F. Sannino, K. Splittorff, Phys.Rev. D65 (2002) 054002.
6. J.B. Kogut, D. Toublan and D.K. Sinclair, hep-lat/0205019.
7. M.-P. Lombardo, Proceedings of *Understanding Deconfinement in QCD*, World Scientific, p.24.
8. K. Splittorff, D. Toublan and J. J. Verbaarschot, Nucl. Phys. B **639** (2002) 524.
9. B. Allés, M. D'Elia, M.-P. Lombardo, M. Pepe, Nucl.Phys.Proc.Suppl.94 (2001) 441.
10. B. Allés, M. D'Elia, M.-P. Lombardo and M. Pepe, to appear.
11. C. DeTar, O. Kaczmarek, F. Karsch and E. Laermann, Phys. Rev. D59(1999) 031501.
12. J. Engels, O. Kaczmarek, F. Karsch and E. Laermann, Nucl. Phys. B558 (1999) 307.
13. F. Gliozzi and P. Provero, Nucl. Phys. B556 (1999) 76.
14. M.-P. Lombardo, J.B. Kogut, D.K. Sinclair, Phys.Rev. D54 (1996) 2303.
15. P.R. Crompton Nucl.Phys.B626 (2002) 228.
16. M.-P. Lombardo, Nucl. Phys. B *Proc. Suppl.* 83(2000)375; Ph. de Forcrand and O. Philipsen, hep-lat/0205016; M. D'Elia and M.-P. Lombardo, hep-lat/0205022; hep-lat0209146.
17. A. Papa e P. Giudice, in progress, private communications.